Supplement of Clim. Past, 17, 151–170, 2021
https://doi.org/10.5194/cp-17-151-2021-supplement

Climate of the Past
Open Access
EGU

Supplement of

El Niño–Southern Oscillation and internal sea surface temperature variability in the tropical Indian Ocean since 1675

Maike Leupold et al.

Correspondence to: Maike Leupold (maike.leupold@emr.rwth-aachen.de)

Introduction. This file includes supplementary methods, pictures of sampling locations (Fig. S1), X-ray images of the coral samples (Fig. S2), photomicrographs of the coral samples (Figs. S3-S5), power spectrum analysis plots of non-detrended coral SST anomalies (Fig. S6), wavelet power spectra of all coral records (Fig. S7), plots with Sr/Ca-SST anomalies and anomalies after detrending (Fig. S8), singular spectrum analysis (SSA) plots (Figs. S9-S11) and power spectrum analysis plots of detrended coral SST (Fig. S12) including text descriptions. Two additional tables giving the years of El Niño and La Niña events used for the composite maps (Table S1) and the linear regression results between the coral SST records and the Wilson Niño Index (Table S2) are also part of this supplementary material.

1 Supplementary Methods

Indices

We use Niño 3.4 SST anomalies taken from NOAA ERSSTv5 (Huang et al. 2017) for power spectrum analysis (Fig. S12). These have been interpolated from sparse observational data and extend back until 1870.

Statistics

Power spectra analysis was performed twice using the spectral analysis function REDFIT (Welch window) of the open source software *PAST* (version 3.25; Hammer et al., 2001). One run was performed with the time series before detrending, one run after detrending. Every time series was detrended using the softwares *breakfit* (Mudelsee, 2009) or *rampfit* (Mudelsee, 2000), respectively (Fig. S8).

SSA (Vautard and Ghil, 1989) were generated using the *MATLAB* (version R2019b) software toolboxes by Groth and Ghil (2015).

2 Table with years of events that were used in the composite maps (Fig. 2 of the main document)

Event years	
El Niño	La Niña
1982/83	1984/85
1986/87	1988/89
1987/88	1995/95
1991/92	1998/99
1994/95	1999/00
1997/98	2007/08
2002/03	2010/11
2009/10	2011/12
2015/16	

Table S1: El Niño and La Niña event years used for the composite maps. Between 1982 and 2016, 9 El Niño events and 8 La Niña events occurred. Temperature anomalies from December to February were averaged for each event.

3 Pictures of coral sample sites

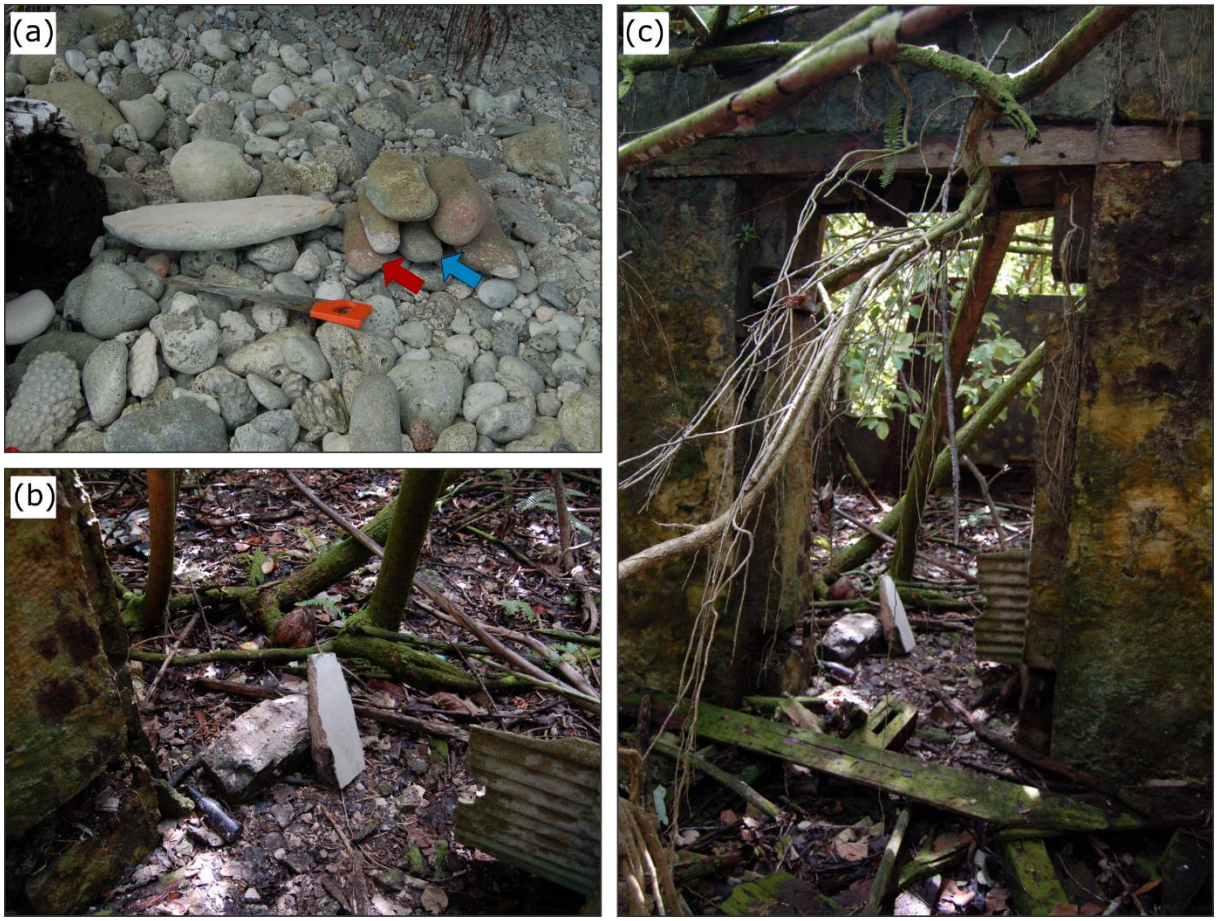

Figure S1: Pictures of coral sample sites. (a) Boulder beach at Eagle Island where the samples E5 (1675-1716; blue arrow) and E3 (1870-1909; red arrow) were collected. (b) and (c) a derelict building at Boddam Island from which the sample B8 (1836-1867) was collected.

4 X-ray images

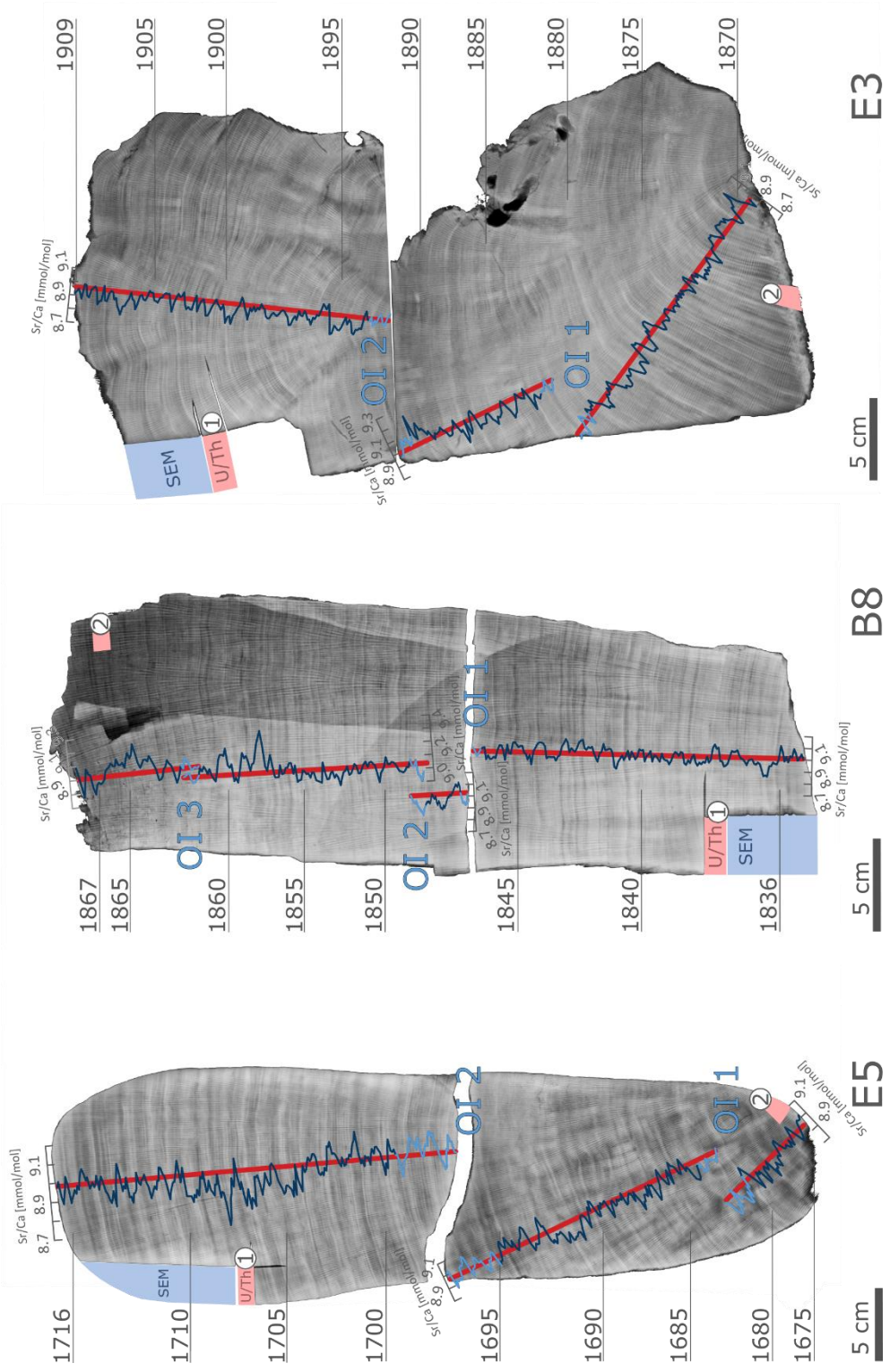

Figure S2: X-ray images of coral samples analyzed in this study with raw Sr/Ca data (dark blue lines with overlapping intervals (OI) in light blue). Age models were interpreted using two U/Th measurements from each sample (sampling points for U/Th dating are indicated with circled numbers and light red-shaded areas; for determined ages see Table 1). Red lines indicate subsampling paths. Blue-shaded areas indicate sampling locations for subsamples used for Scanning Electron Microscopy (SEM). Please note that the slab of sample B8 is uneven as the slab was too brittle to polish out saw cuttings from field work and these are still seen on the X-ray image. Note the even growth patterns of all samples.

5 Thin section and SEM analysis images

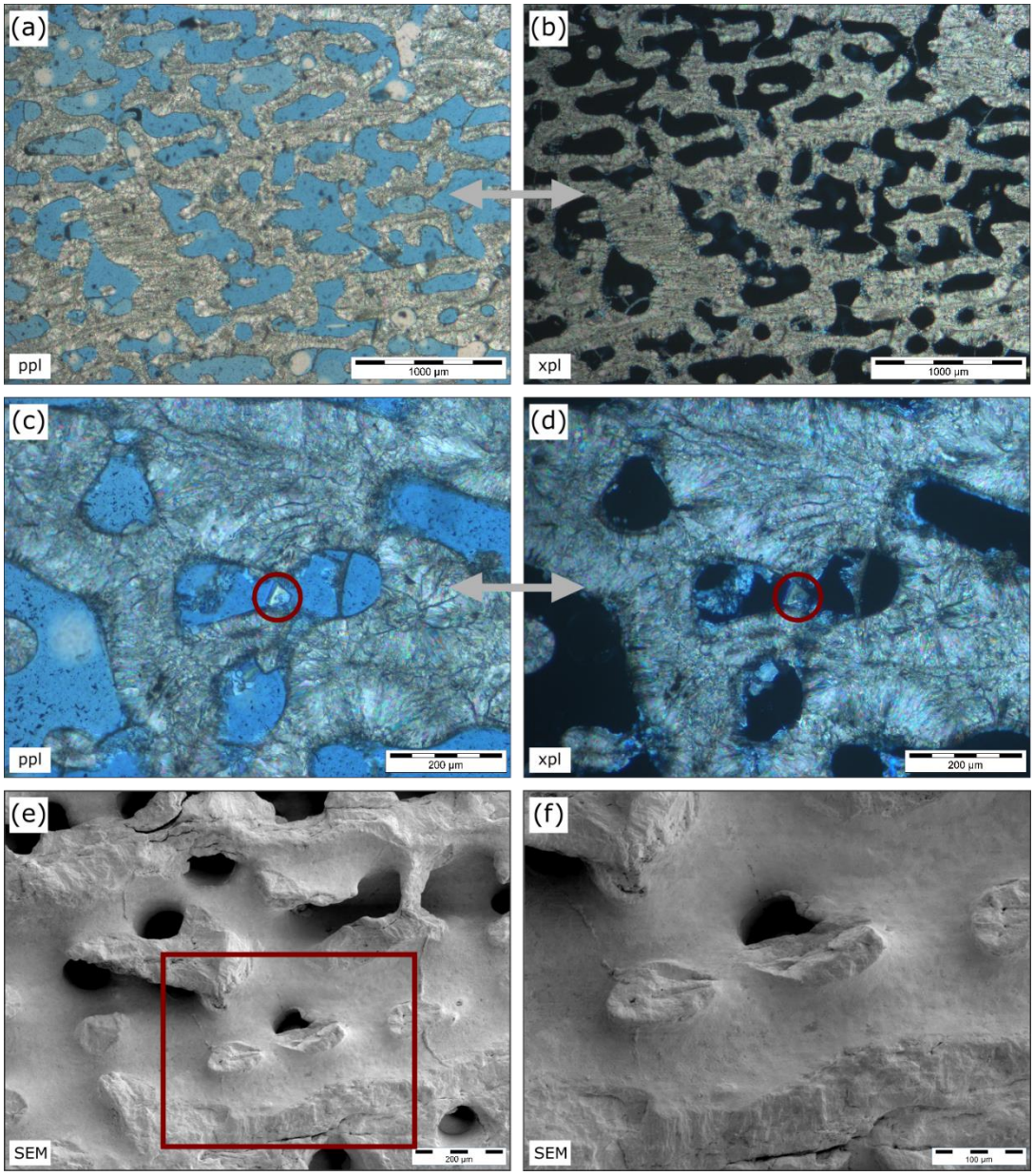

Figure S3: Photomicrographs of coral sample E5 (1675-1716). Double arrows indicate corresponding photomicrographs. (a) PPL and (b) XPL overview photomicrograph of the coral skeleton. (c) PPL and (d) XPL photomicrograph of the sample at higher resolution where minor amounts of secondary calcite cement are visible (red circle). (e) SEM overview and (f) detail image (red box in e) where only trace amounts of sugary cements can be found.

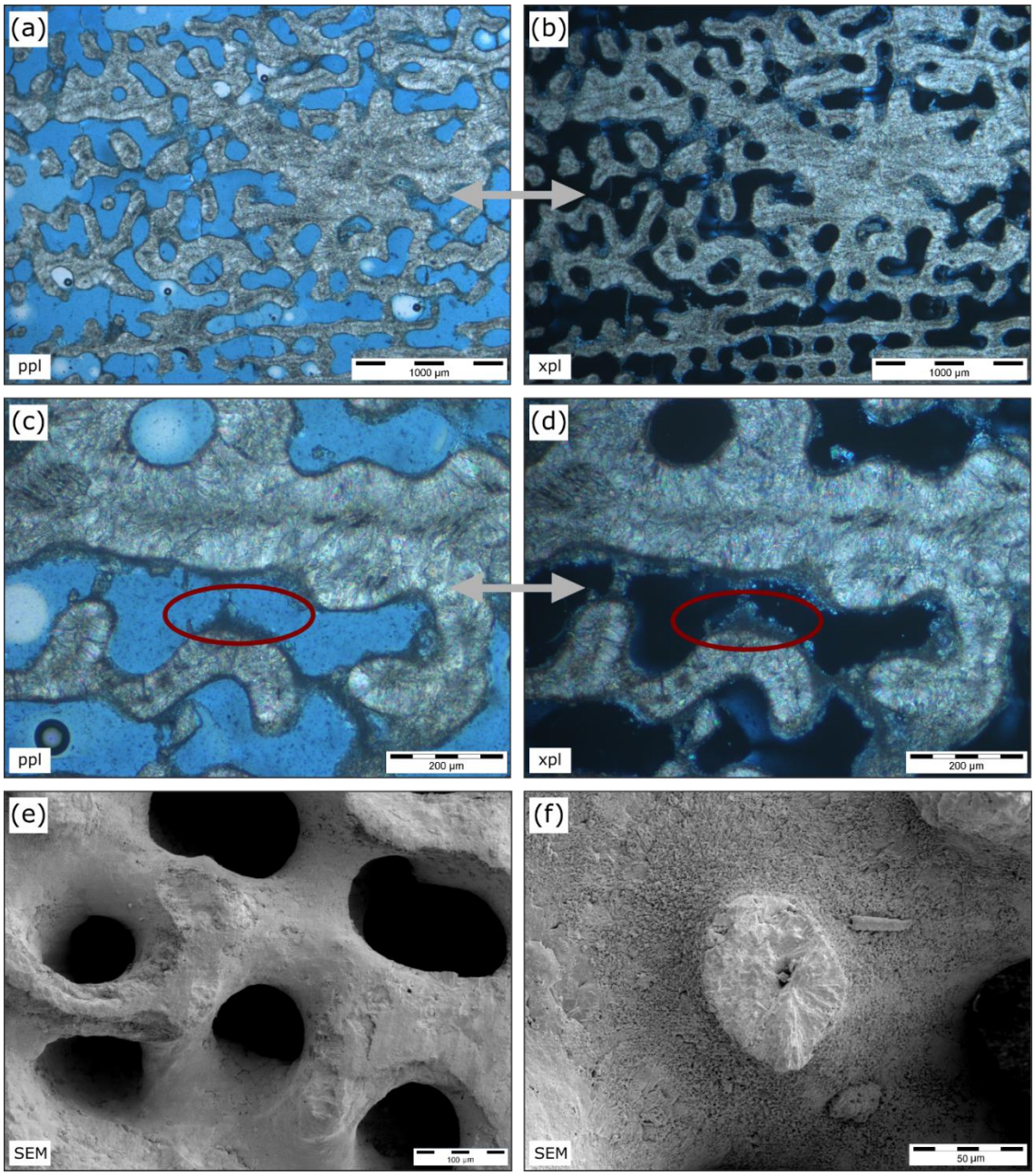

Figure S4: Photomicrographs of coral sample B8 (1836-1867). Double arrows indicate corresponding photomicrographs. (a) PPL and (b) XPL overview photomicrograph of the coral skeleton. (c) PPL and (d) XPL photomicrograph of the sample at higher resolution where small amounts of secondary aragonite cement are visible (red oval). (e) SEM overview and (f) detail image of B8 (1836-1867). Small amounts of sugary aragonitic cement can be seen.

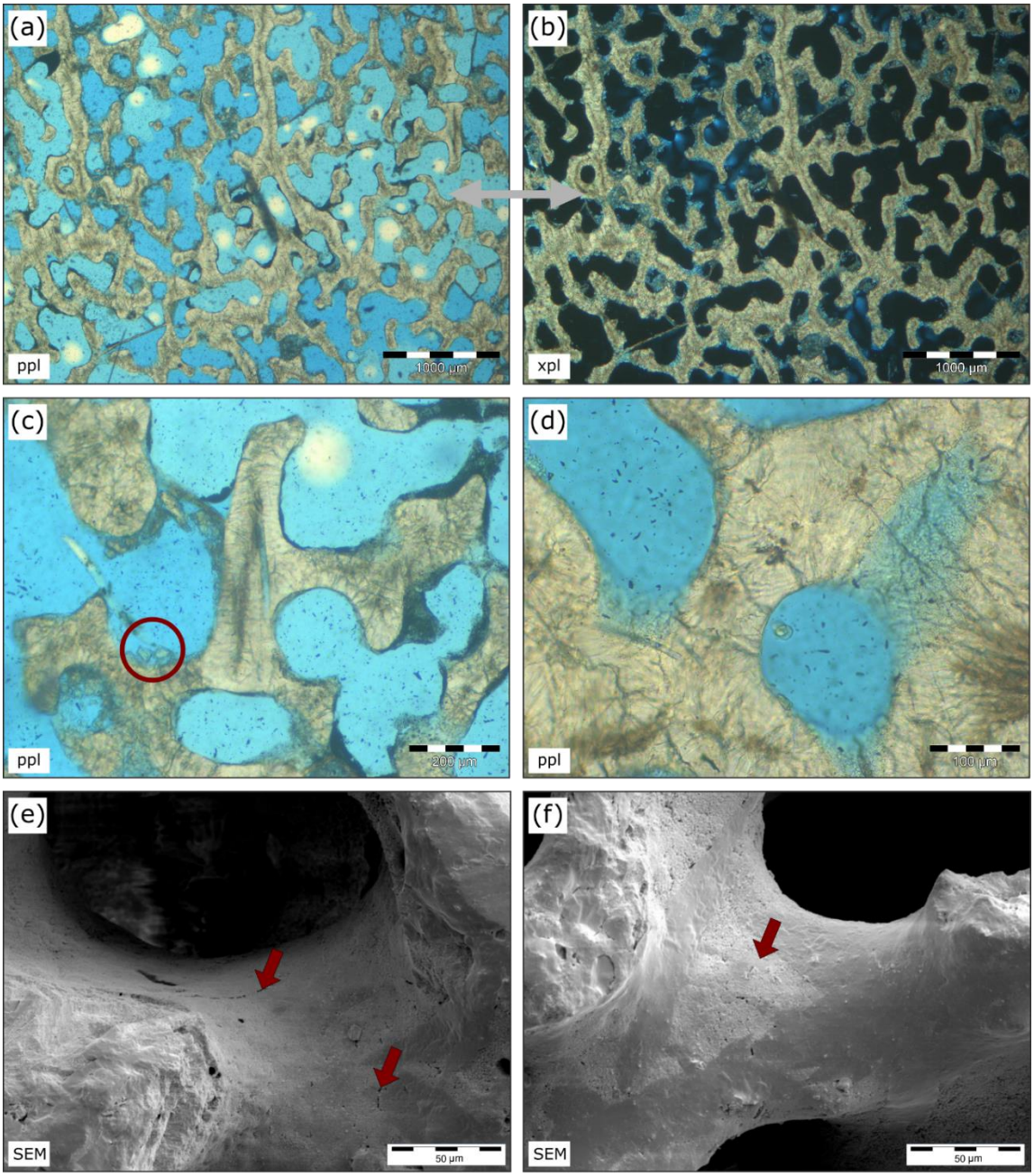

Figure S5: Photomicrographs of coral sample E3 (1870-1909). Double arrows indicate corresponding photomicrographs. (a) PPL and (b) XPL overview photomicrograph of the coral skeleton. (c) PPL photomicrograph of the sample at higher resolution where small fragments of aragonite are found (red circle). (d) PPL microphotograph of the sample at higher resolution without any signs of diagenesis. SEM images showing (e) microborings (red arrows) and (f) areas which appear brighter due to dissolution.

6 Seasonal cycles inferred from Singular Spectrum Analysis

Singular spectrum analysis (SSA) of the coral records with seasonal cycles reveal large interannual to decadal SST variabilities during both the 17-18th century and 19-20th century (not shown). The reconstructed components 2 and 3 (RC2, RC3) produced by SSA describe seasonal amplitudes for all samples and explain 28% (E5), 26% (B8), 32% (E3) of the coral Sr/Ca-SST variance. Decadal variabilities are larger during the 17-18th century compared to the 19-20th century. The first reconstructed component (RC1) of E5 with seasonal cycles explains 48% of the coral Sr/Ca-SST variance and describes a periodicity of around 18 years. The coral records covering the 19-20th century do not show a strong decadal component in SSA. Instead, RC1 explains 49% (B8) and 39% (E3) of the coral Sr/Ca-SST variance and describes a periodicity of around 7 years, which can be interpreted as ENSO periodicity.

The SSA results were validated by power spectrum analysis of bimonthly resolved coral SST anomalies, which were not detrended (Fig. S6). For this analysis, the coral record GIM (Pfeiffer et al., 2017) was included, which extends from 1880 to 1995. Power spectrum analysis of E5 (Fig. S6a) shows a low-frequency band corresponding to a periodicity of 18-19 years, identical to RC1 of the SSA. In addition, RC2 describing an ENSO periodicity of 4-5 years is confirmed by the second highest low-frequency band in power spectrum analysis of E5. The power spectrum analysis of the corals covering the 19-20th century (B8 and E3) confirms their SSA results, as well (Figs. S6b & c). It shows high power on the low-frequency (5-6 years for B8; 6-7 years for E3) band, which was also described by the first reconstructed components in SSA. Power spectrum analysis for GIM (Fig. S6d) reveals high power on the ENSO band (4-5 years and 8 years) and the highest power at the decadal frequencies (26 years).

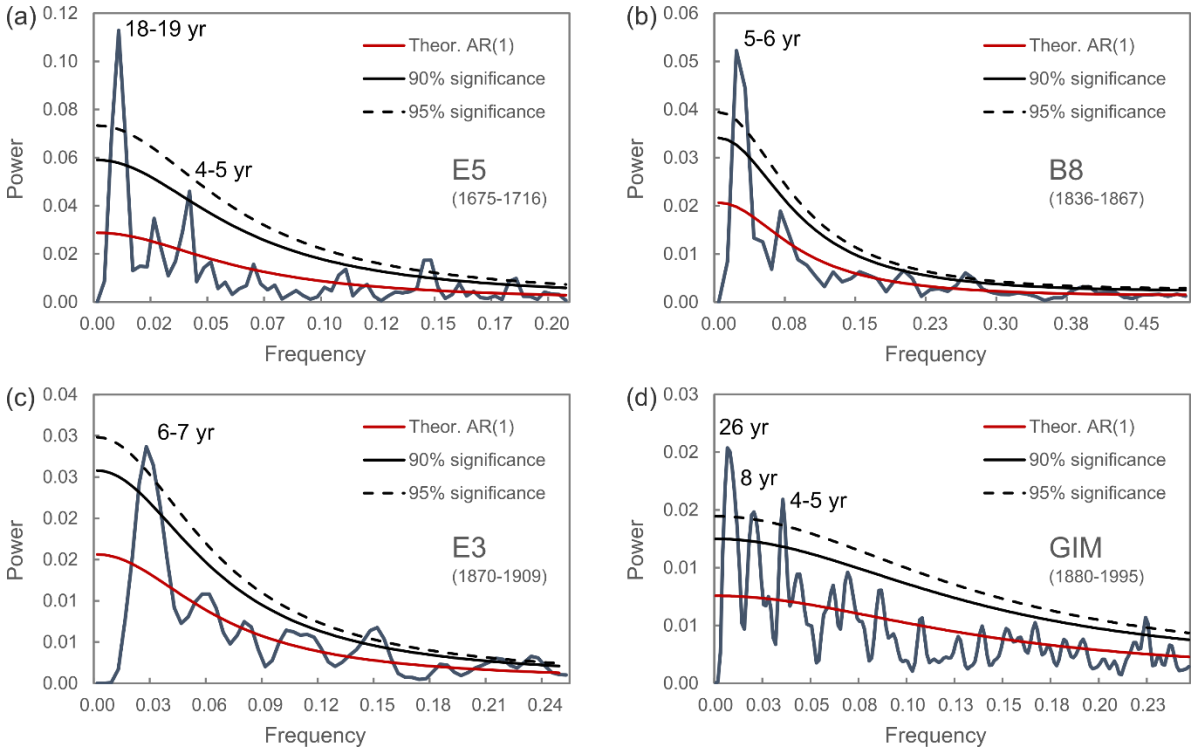

Figure S6: Power spectrum analysis of each Chagos coral bimonthly resolved anomaly series.

7 Wavelet Power Spectra

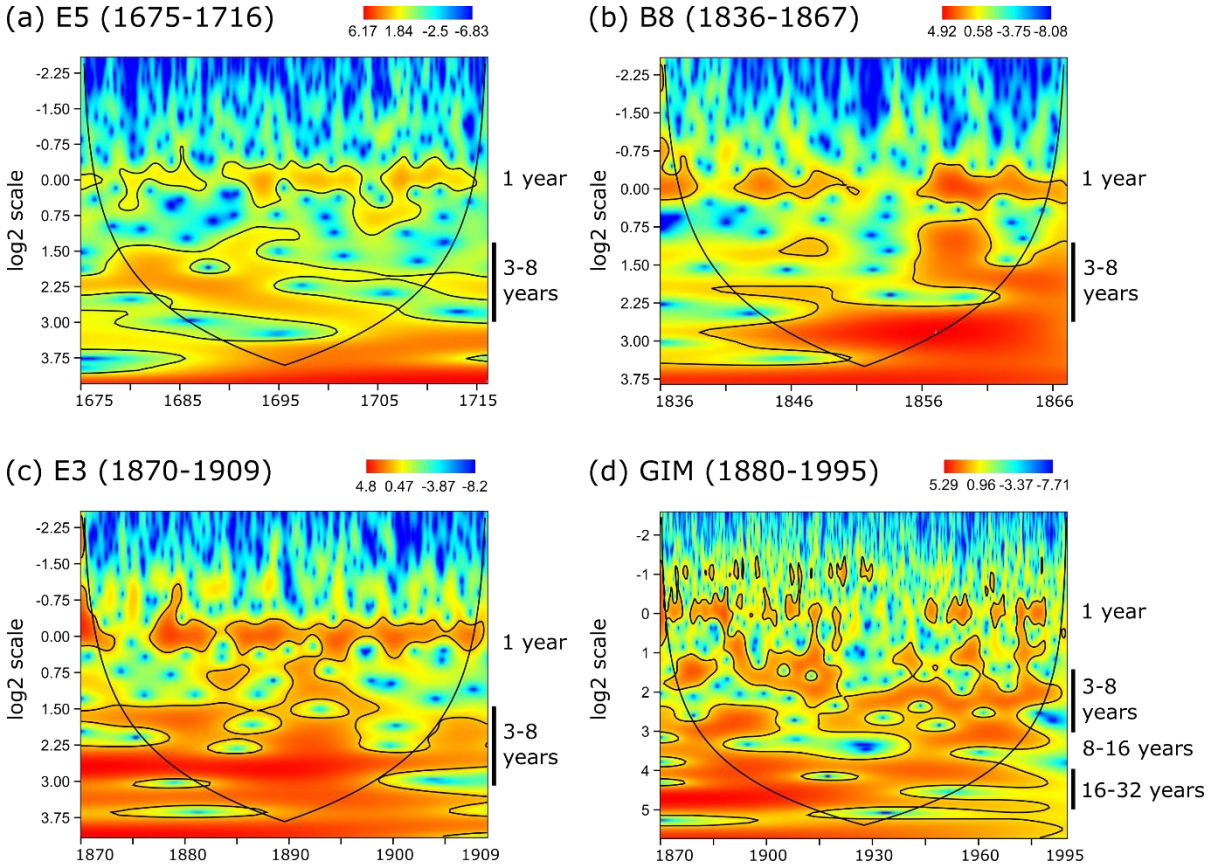

Figure S7: Wavelet power spectra of (a) E5 (1675-1716), (b) B8 (1836-1867), (c) E3 (1870-1909) and (d) GIM (1880-1995) coral Sr/Ca records. Wavelet power spectra were computed using the Morlet wavelet. The cone of influence and the 95% confidence level are indicated by the black lines. All spectra were computed with the free software package PAST (version 3.25; Hammer et al., 2001).

8 Detrending of coral SST records

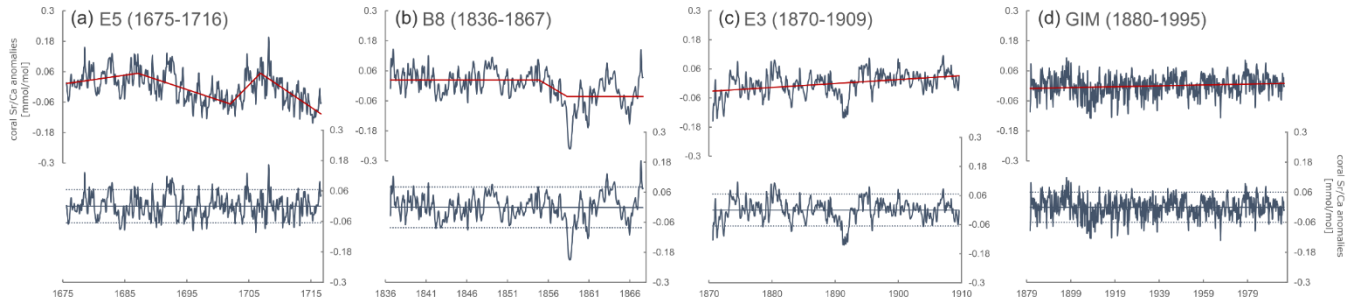

Figure S8: Sr/Ca-SST anomalies with calculated trend lines (red lines; upper plot) and anomalies after detrending (lower plot; with plotted 1.5x of the standard deviation as dashed lines) for the coral records (a) E5 (1675-1716), (b) B8 (1836-1867), (c) E3 (1870-1909) and (d) GIM (1880-1995).

9 Interannual SST variability inferred from Singular Spectrum Analysis

The spectral results of the coral records with seasonal cycles were validated by singular spectrum analysis (SSA) of coral SST anomalies records and power spectrum analysis, to reveal stronger patterns of variance when seasonal cycles were subtracted (Figs. S9-S12). During the 17-18th century, the coral record shows a periodicity of 18 years in RC1, which explains 47% of the coral Sr/Ca-SST variance (Fig. S9). The second reconstructed component (RC2; Fig. S9) of E5 (1675-1716) explains 14% of the coral Sr/Ca-SST variance and describes an ENSO periodicity of 4-5 years. During the 19-20th century, the pattern of variance describing the ENSO periodicity in the coral records are found in two to three reconstructed components: For B8 (1836-1867), RC2 and RC3 describe an ENSO periodicity of 5-8 years with in total 62% of the corals Sr/Ca-SST variability (Fig. S10). For E3 (1870-1909) it is even higher with RC1-3 explaining 65% of the coral Sr/Ca-SST variance. Those three components describe a characteristic ENSO periodicity of 3-8 years (Fig. S11).

Power spectra of detrended coral SST time series all show the typical ENSO periodicity between 3 and 8 years (Fig. S12a-d). Those periodicities can also be found in the power spectra of the Niño3.4 indices (Fig. S12e & f). Even after detrending, the power spectrum of the GIM coral SST record still shows the highest power at low-frequencies, which translates to a period of 21-22 years.

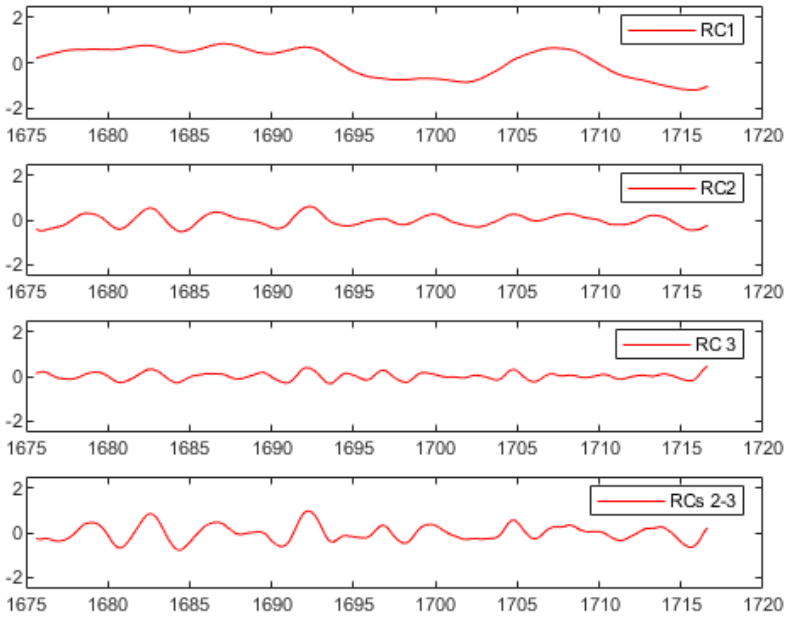

Figure S9: Reconstructed components from Singular Spectrum Analysis of E5 (1675-1716) Sr/Ca monthly anomalies. First reconstructed component (RC1) describes a periodicity of 18 years. RC2 and RC3 describe typical ENSO periodicities.

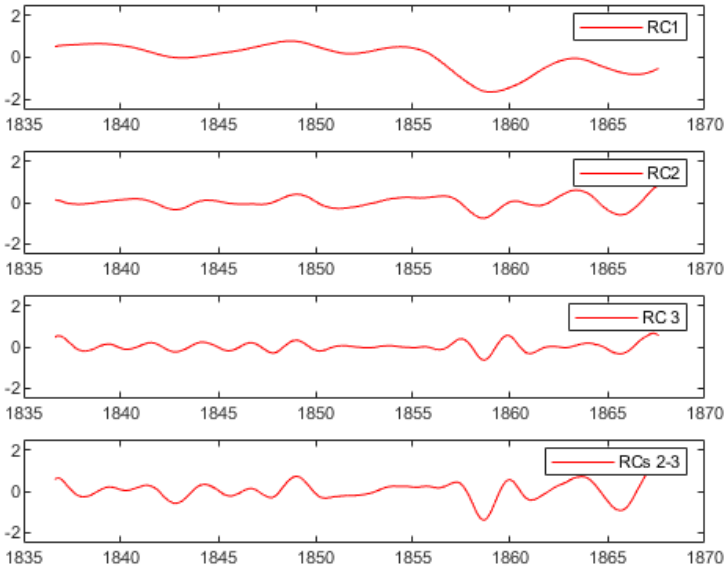

Figure S10: As Figure S9, but for coral Sr/Ca record of B8 (1836-1867).

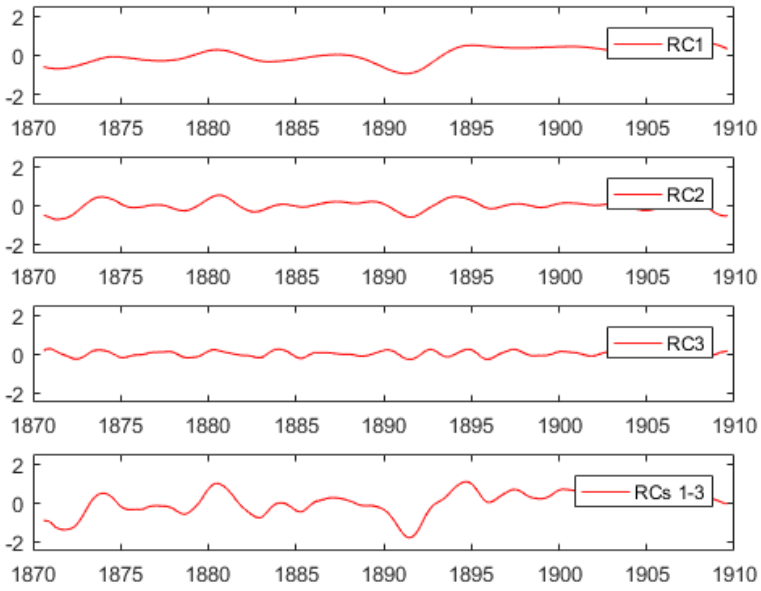

Figure S11: As Figures S9 and S10, but for coral Sr/Ca record of E3 (1870-1909). ENSO periodicities are described by all shown reconstructed components RC1-3.

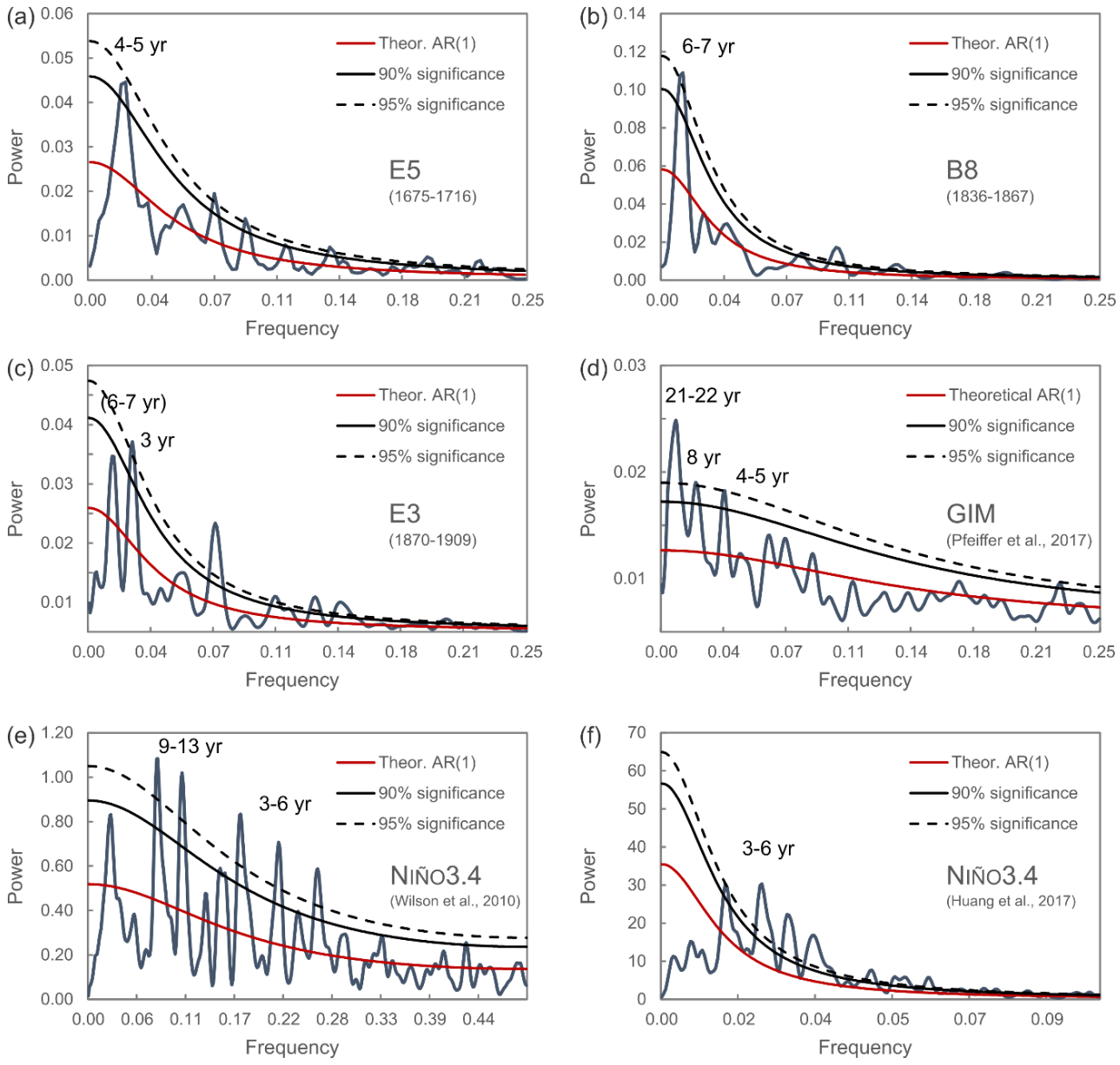

Figure S12: Power spectrum analysis plots for detrended coral SST, the annually resolved Wilson Niño index (Wilson et al., 2010) and the monthly resolved Niño3.4 index based on NOAA ERSSTv5 (Huang et al., 2017) time series.

10 Linear regression

Ordinary least square (OLS) regression and *PearsonT3* calculation results reveal no significant linear relation between annual coral SST records and the Wilson Niño index (Table S2).

Method	Coefficient	E5 (1675-1716)	B8 (1836-1867)	E3 (1870-1909)	GIM (1880-1995)
Excel OLS	R^2 (p-value)	4.09E-5 (0.9679)	0.0006 (0.8979)	0.0027 (0.7502)	0.0444 (0.0232)
PearsonT3	r [95% confidence interval]	-0.006 [-0.361; 0.350]	-0.024 [-0.739; 0.716]	0.052 [-0.418; 0.500]	0.211 [-0.005; 0.408]

Table S2: Correlation coefficients of given coral records with the Wilson Niño index.

Supplementary References

Groth, A., and Ghil, M.: Monte Carlo Singular Spectrum Analysis (SSA) revisited: Detecting oscillator clusters in multivariate datasets, J. Climate, 28, 7873-7893, https://doi.org/10.1175/JCLI-D-15-0100.1, 2015.

Hammer, Ø., Harper, D. A. T., and Ryan, P. D.: Paleontological statistics software: package for education and data analysis, Palaeontol. Electron., (4), 2001.

Huang, B., Thorne, P. W., Banzon, V. F., Boyer, T., Chepurin, G., Lawrimore, J. H., ... and Zhang, H. M.: Extended reconstructed sea surface temperature, version 5 (ERSSTv5): upgrades, validations, and intercomparisons, J. Climate, 30(20), 8179-8205, https://doi.org/10.1175/jcli-d-16-0836.1, 2017.

Mudelsee, M.: Ramp function regression: A tool for quantifying climate transitions, Comput. Geosci.-UK, 26(3), 293-307, https://doi.org/10.1016/s0098-3004(99)00141-7, 2000.

Mudelsee, M.: Break function regression: A tool for quantifying trend changes in climate time series, Eur. Phys. J.-Spec. Top., 174(1), 49-63, https://doi.org/10.1140/epjst/e2009-01089-3, 2009.

Pfeiffer, M., Zinke, J., Dullo, W. C., Garbe-Schönberg, D., Latif, M., and Weber, M. E.: Indian Ocean corals reveal crucial role of World War II bias for twentieth century warming estimates, Sci. Rep.-UK, 7(1), 14434, https://doi.org/10.1038/s41598-017-14352-6, 2017.

Vautard, R., and Ghil, M.: Singular spectrum analysis in nonlinear dynamics, with applications to paleoclimatic time series, Physica D, 35, 395-424, https://doi.org/10.1016/0167-2789(89)90077-8, 1989.

Wilson, R., Cook, E., D'Arrigo, R., Riedwyl, N., Evans, M. N., Tudhope, A., and Allan, R.: Reconstructing ENSO: the influence of method, proxy data, climate forcing and teleconnections, J. Quaternary Sci., 25(1), 62-78, https://doi.org/10.1002/jqs.1297, 2010.